A Gustotopic Map of Taste Qualities in the Mammalian Brain

Xiaoke Chen,[1] Mariano Gabitto,[1] Yueqing Peng,[1] Nicholas J. P. Ryba,[2] Charles S. Zuker[1,3]*

The taste system is one of our fundamental senses, responsible for detecting and responding to sweet, bitter, umami, salty, and sour stimuli. In the tongue, the five basic tastes are mediated by separate classes of taste receptor cells each finely tuned to a single taste quality. We explored the logic of taste coding in the brain by examining how sweet, bitter, umami, and salty qualities are represented in the primary taste cortex of mice. We used in vivo two-photon calcium imaging to demonstrate topographic segregation in the functional architecture of the gustatory cortex. Each taste quality is represented in its own separate cortical field, revealing the existence of a gustotopic map in the brain. These results expose the basic logic for the central representation of taste.

The sense of taste is in charge of evaluating the nutritional value of a meal. In mammals, a very small palette of taste qualities orchestrates appetitive responses to energy- and protein-rich food sources (sweet and umami) and warns against the ingestion of toxic or spoiled/fermented foods (bitter and sour/carbonated). Salt sensing aids the adequate consumption of sodium while cautioning against the ingestion of excess salt. The attraction toward sweet, umami, and low-sodium, and the aversion toward bitter, sour, and high-salt, is innate and largely invariant throughout life. These observations suggest a physiological hard-wiring of tastant quality to hedonic value.

Each of the five basic tastes is detected by specialized sensors expressed on receptor cells of the tongue and palate epithelium (*1*–*11*). Over the past 10 years, we have shown that each receptor class is expressed in its own distinct taste cell type (*2*–*6*, *8*, *12*, *13*). This "one cell, one taste" coding scheme is the hallmark of the organization of the mammalian taste system at the periphery, and is the mechanism through which individual taste qualities are recognized and encoded in the tongue (*9*, *14*).

In rodents, information from taste cells in the oral cavity is transmitted to the primary taste cortex, the insula, through multiple neural stations (*14*, *15*). How are the chemical senses represented in the cortex? Recent studies on the representation of odors in the primary olfactory cortex revealed a sparse and distributed pattern of neuronal activity whereby each odor is encoded by a unique ensemble of neurons, but without any spatial clustering or preference in relation to odorant space (*16*). This is in contrast to the organization of the primary visual, somatic, and auditory cortices, where neurons that respond to similar features of the sensory stimulus are topographically organized into spatial maps in the cortex (*17*–*19*).

Previous studies examining how tastes are represented in the primary gustatory cortex have relied on a number of elegant approaches (*20*–*25*). Unfortunately, these experiments have led to inconclusive and often contradictory views of the central representation of taste, in part because of the limited spatial resolution of the techniques and/or the shortfalls of recording from small numbers of neurons (*15*, *26*). We reasoned that if one could simultaneously examine the activity of large numbers of neurons in the insular cortex in response to taste stimulation (*27*), and do so with single-cell resolution, it should be possible to determine how the tastes are represented in the primary taste cortex.

Imaging gustatory responses in the primary taste cortex. We used two-photon calcium imaging (*16*, *28*–*30*) to monitor tastant-evoked neural activity across the gustatory cortex in vivo. To confirm the appropriate region for imaging in mice (*20*, *25*), we used extracellular electrodes to record tastant-evoked responses in the gustatory area of the thalamus (Fig. 1), and after identifying taste-responding cells, we used an AAV2/hu11-GFP virus (*31*) as an anterograde tracer to label (and trace) projections to the primary taste cortex (Fig. 1C) (*32*). These studies demarcated a domain of ~2.5 mm^2 in the insula, located ~1 mm above the intersection of the middle cerebral artery (MCA; Fig. 1, A and C) and the rhinal veins, and extending ~1 mm anteriorly, 1.5 mm posteriorly, and 1 mm dorsoventrally. Small areas of cortex were exposed in this region of the insula of anesthetized animals (via surgical craniotomy), and the neurons were bulk-loaded with the calcium-sensitive dye Oregon Green 488 BAPTA-1 AM (OGB) for functional imaging (Fig. 1D); this dye is effectively taken up by the cells (fig. S1) and serves as a robust fluorescent sensor of neural activity with high signal-to-noise ratios (*16*, *29*, *30*). To ensure that responses reflected biologically relevant stimuli, we used concentrations of tastants that reliably elicit ~80% of the maximal response in behavioral studies (*3*, *8*).

Representation of bitter taste. We systematically inspected layer 2/3 of the gustatory cortex (a layer readily accessible by two-photon imaging) for tastant-evoked responses by parsing and tiling the insula into fields of 350 μm × 350 μm and testing for neurons that exhibited correlated patterns of tastant-dependent firing (*16*). The stimulus paradigm consisted of a prestimulus application of artificial saliva for 30 s, exposure to a test tastant for 10 s, and a poststimulus artificial saliva wash for 30 s (*32*). We began by focusing on bitter taste, and discovered a highly localized, topographically defined cluster (i.e., a "hot spot" at ~1 mm dorsal to the rhinal veins and ~1 mm posterior to the MCA) (*32*), where many neurons responded to bitter stimuli with highly significant increases in intracellular calcium ($\Delta F/F$ ranging from 20 to 65%; Fig. 2); the location of the hot spot was stereotyped so that we could consistently find this cortical field in multiple animals (Fig. 2F and fig. S2). We examined the reproducibility of the taste-evoked responses in the hot spot by measuring variability across trials. We imaged ~200 neurons per trial, and these were segmented and coded according to their location and response magnitude (*16*, *33*). On average, about one-third of the OGB-labeled neurons fired during the window of bitter tastant application, and the vast majority of these (>70%) responded in multiple bitter-stimulation trials (compare Fig. 2A and 2B; see also fig. S3). By examining bitter responses across the entire gustatory cortex in multiple animals, we confirmed this hot spot (i.e., cortical field) as the only region that exhibited correlated responses to bitter stimuli (Fig. 2F and fig. S2).

Are the bitter-responsive neurons selective or broadly tuned? We recorded from the bitter hot spot while stimulating the tongue with tastants representing the different taste qualities. Bitter-responding neurons were exquisitely tuned to bitter, with no other taste quality represented in this spatial domain of the gustatory cortex (Fig. 2). Equivalent results were obtained in single-unit electrophysiological recordings from within the bitter hot spot (fig. S4).

Humans and rodents recognize a wide range of bitter tasting chemicals, and their genomes correspondingly include a large number of genes that encode bitter taste receptors (T2Rs) (*5*–*7*). Most, if not all, T2Rs are expressed in the same subset of taste receptor cells (*5*), implying that these cells act as broadly tuned bitter sensors capable of detecting a wide range of bitter-tasting chemicals (*5*, *8*). Thus, we predicted that the cortical representation for different bitter tastants should be shared. We therefore assayed the responses to several chemically distinct bitter tastants, and indeed all of them activated the same hot spot (Fig. 3 and fig. S3).

Specificity of cortical responses to taste stimuli. To further validate the specificity of the bitter cortical field, we examined taste responses in engineered mice where a single one of the

[1]Howard Hughes Medical Institute, Department of Biochemistry and Molecular Biophysics, and Department of Neuroscience, College of Physicians and Surgeons, Columbia University, New York, NY 10032, USA. [2]National Institute of Dental and Craniofacial Research, Bethesda, MD 20892, USA. [3]Departments of Neurobiology and Neurosciences, University of California, San Diego, La Jolla, CA 92093, USA.

*To whom correspondence should be addressed. E-mail: cz2195@columbia.edu

bitter taste receptors had been eliminated. T2R5 is one of the 36 bitter receptors in the mouse genome (*34*); it is necessary (and sufficient) for physiological and behavioral taste responses to the toxin cycloheximide, but not for detecting a wide range of other bitter chemicals (*6*, *8*). If the bitter-evoked activity in the hot spot is indeed used to represent bitter taste, then all responses to cycloheximide should be missing in a T2R5 knockout (T2R5-KO) animal. However, responses to other bitter tastants should remain. This selective-loss experiment alleviates the uncertainty associated with examining animals with a total loss of bitter taste [e.g., TRPM5 or PLCβ2 knockouts (*13*)], as such a negative result could not be distinguished from a trivial failure to record cortical responses. As predicted, cycloheximide responses were abolished in the bitter hotspot of T2R5-KO animals, but responses to other bitter chemicals were indistinguishable from those in control mice (Fig. 3).

A spatial map of taste qualities. Given the existence of a topographically defined region for the representation of bitter taste, we hypothesized that sweet taste would also be encoded in its own cortical field, and therefore surveyed the insular cortex for selective activity to sweet tastants. We discovered such a specific sweet hot spot at a considerable distance from the bitter hot spot (~2.5 mm rostrodorsal to the bitter field; Fig. 4, A and B). There, a large ensemble of neurons responded to sweet taste stimulation of the tongue. Multiple lines of evidence validate that area as the sweet cortical field: First, the cells were preferentially tuned to sweet taste versus any of the other taste qualities (Fig. 4B and fig. S5). Second, the very same hot spot was activated by structurally different sweet-tasting chemicals (e.g., artificial versus natural sweeteners), but not by tastants for other taste qualities (Fig. 4, A and B, and fig. S5). Third, responses were abolished in sweet-receptor knockout animals [T1R2-KO (*3*); fig. S6]. Finally, this is the only region of gustatory insula that showed correlated activity in response to sweet taste.

The topographic separation of sweet and bitter taste into distinct and nonoverlapping gustatory fields in the primary taste cortex reveals the existence of a functional "gustotopic map." In the other chemosensory modality, olfaction, individual odorants are represented in the primary olfactory cortex by the activation of spatially dispersed ensembles of neurons, without any discernible topographic or chemotopic organization (*16*). However, unlike the olfactory system—which must recognize, distinguish, and often initiate distinct physiological and behavioral responses to a vast universe of chemically distinct odorants—the chemical-perceptual space, represented by the five basic taste qualities, is remarkably limited (*9*, *14*). Sweet and bitter exemplify the two poles of the gustatory spectrum; thus, we wondered whether the other taste qualities were also part of a gustatory map in the insula.

Umami is the savory taste that humans associate with monosodium glutamate (MSG); most other mammalian species use the umami-sensing taste receptor cells to recognize and mediate appetitive responses to protein-rich food sources [e.g., the taste of all amino acids (*1*, *2*, *35*)]. We searched the insular cortex for umami-evoked neuronal activity by stimulating the tongue with monopotassium glutamate (*36*). Indeed, just as seen for bitter and sweet, the cortical representation of umami was also part of the gustotopic map, with a unique hot spot for umami taste (Fig. 4, C and D, and fig. S5). The umami cortical field was specifically tuned to umami versus the other four taste qualities. As expected, this hot spot was activated by other L-amino acids (e.g., umami agonists; Fig. 4D) but not by their enantiomeric inactive D-forms (*2*, *3*).

The remaining two basic tastes, salt (sodium) and sour (acid) sensing, are mediated by ion channel receptors rather than by G protein–coupled receptors (*10*–*12*, *37*). Does the same organization apply to ionic tastes? Our efforts to uncover an acid (sour) hot spot did not succeed. We believe this could be because its location was outside the area sampled in our studies, or even because acid stimuli also act on a number of other pathways, such as pain and somatosensation (*38*), possibly leading to changes in its cortical representation. Thus, we focused on sodium taste.

Low concentrations of NaCl (i.e., appetitive salt taste) are sensed by a unique population of taste receptor cells via the ENaC ion channel (*12*). A salient feature of this response is its inhibition by amiloride and its strong selectivity for sodium versus other salts (*12*). Therefore, we searched for a salt-responsive cortical

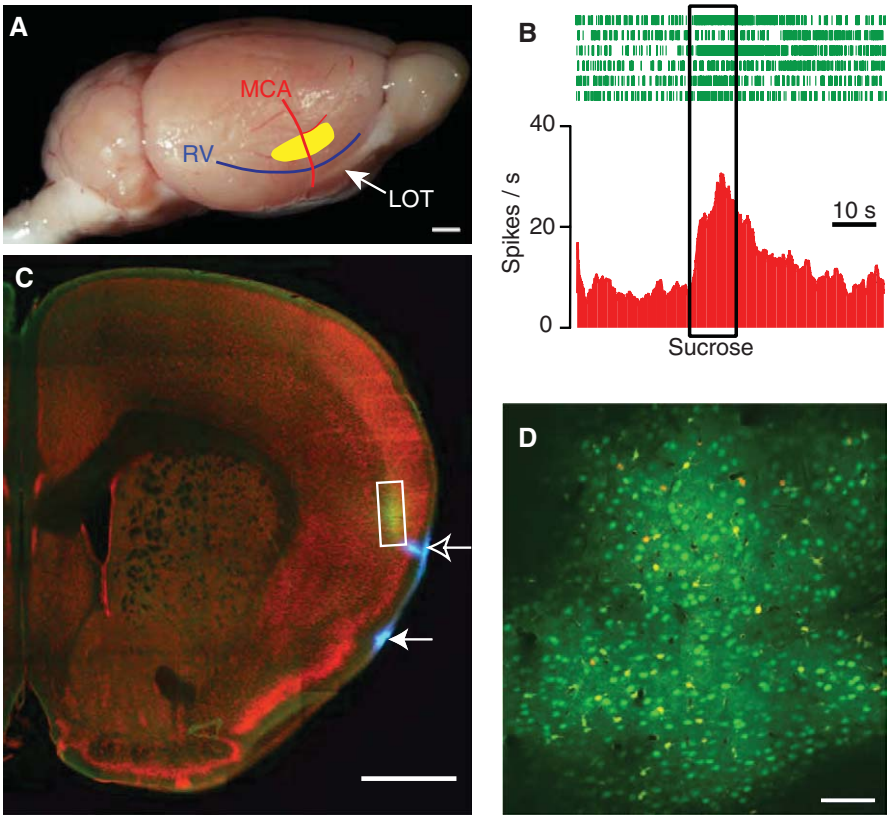

Fig. 1. Two-photon imaging in the mouse insular cortex. (**A**) Photograph of a mouse brain highlighting the approximate location of our imaging studies in the primary taste cortex (yellow). Also shown are the superimposed drawings of two key vascular landmarks (MCA, middle cerebral artery; RV, rhinal vein; LOT, lateral olfactory tract). (**B**) Responses of a sweet-sensitive thalamic taste neuron to 300 mM sucrose; the box indicates the time and duration of the sweet stimulus. After identification of such taste-responsive neurons, cells around the recording site were infected with an AAV2/hu11-GFP virus to label their terminal fields in layer 4 of the gustatory cortex. (**C**) Coronal section of a mouse brain (bregma +1.0) stained with TO-PRO-3 (red). Shown is the location of the thalamocortical projections labeled after infection with the AAV2/hu11-GFP virus (white box). To triangulate this region in relation to the vascular landmarks, we injected 1,1′-dioctadecyl-3,3,3′,3′-tetramethylindocarbocyanine perchlorate (DiI) at the intersection between the RV and the MCA (pseudocolored in blue; solid arrow) and at 1 mm above (open arrow). (**D**) Images of bulk-loaded neurons and astrocytes in layer 2/3 of the primary gustatory cortex (see also fig. S1) stained with Oregon Green 488 BAPTA-1 AM (green fluorescence) and sulforhodamine 101 (yellow-labeled astrocytes). Animals were imaged using two-photon microscopy in vivo after surgical craniotomy. Scale bars, 1 mm [(A) and (C)], 100 μm (D).

cluster that met those criteria. Just as shown for the other basic taste qualities, sodium taste is also represented in its own spatially segregated field (Fig. 4, E and F, and fig. S5). The responding neurons are exquisitely tuned to NaCl versus the other taste qualities, are sensitive to amiloride, and are specific for sodium versus other cations (e.g., KCl, $MgCl_2$).

Concluding remarks. For many years, the prevailing views about the organization and function of the taste system at the periphery centered around the concept of taste coding via broadly tuned taste receptor cells (*39*–*41*). Individual taste receptor cells were proposed to express receptors for various taste qualities and thus respond to multiple taste stimuli. Now, however, we know that each of the five basic tastes is mediated by its own class of taste receptor cells, each tuned to a single taste quality, thus defining a "one cell, one taste" coding logic (*9*, *14*). Notably, existing models of taste coding in the insula included proposals of broadly tuned neurons across taste qualities [with no spatial segregation (*15*)], as well as others suggesting a certain degree of topographic organization, but with no region dedicated to the processing of only one taste quality (*20*, *25*, *26*). Although we cannot rule out the existence of sparse numbers of broadly tuned cells (*24*, *26*) distributed throughout the taste cortex (i.e., nonclustered), our results reveal that

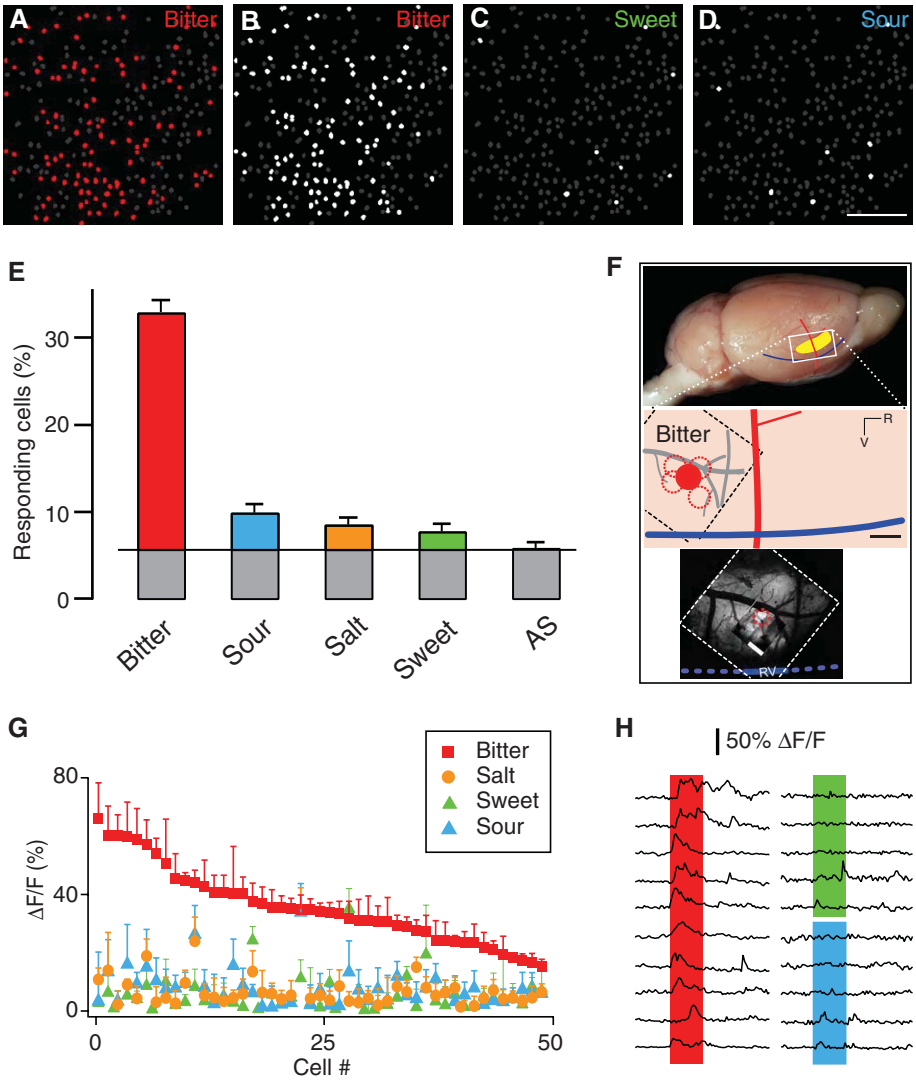

Fig. 2. Tastant-evoked responses in the bitter hot spot. (**A**) Bitter tastant stimulation of the tongue (single trial) evoked robust responses in the bitter hot spot. The image illustrates changes in OGB fluorescence in response to a 1 mM cycloheximide stimulus; ~35% of the loaded neurons responded with $\Delta F/F$ greater than 3.5 standard deviations above background (red cells; see also fig. S7). (**B** to **D**) In contrast to the sparse activity seen during application of other tastants [(C) and (D); see text], neurons activated by bitter tastant responded over multiple trials; cells that responded in at least two of four trials are labeled white (B). (**E**) Neurons in the bitter hot spot responded selectively to bitter versus other taste stimuli (n = 8). AS, artificial saliva. (**F**) An illustration and a bright-field image depicting the approximate relation of the bitter cortical field (solid red circle) to the vascular landmarks; the dotted circles depict the location of the bitter hot spot in four additional animals (*32*). The middle panel has been flattened to present a two-dimensional view of this area of the brain. (**G**) Bitter-responsive neurons are highly tuned to bitter taste (red). The graph shows the rank-ordered $\Delta F/F$ of a set of bitter-responsive neurons in a six-trial experiment to bitter stimuli versus other tastants (bitter = 1 mM cycloheximide; NaCl = 100 mM NaCl; sweet = 30 mM acesulfame K; sour = 10 mM citric acid). No apparent organization according to response amplitude was seen within the cluster (fig. S8). (**H**) Representative changes in OGB fluorescence during bitter (red), sweet (green), and sour (blue) stimulation for 10 s. Scale bars: 100 μm [(A) to (D)], 0.5 mm (F); error bars are means ± SEM.

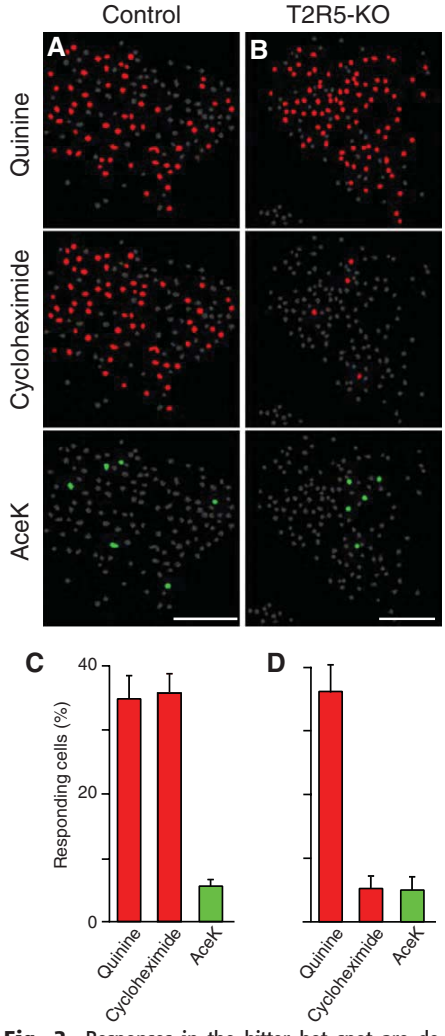

Fig. 3. Responses in the bitter hot spot are dependent on bitter taste receptor function. (**A**) Different bitter compounds activate the same hot spot in the cortex (see fig. S3) (n = 4). (**B**) Animals lacking the bitter taste receptor for cycloheximide (T2R5-KO) selectively lack cortical responses to cycloheximide but retain normal responses to other bitters (e.g., 10 mM quinine) (n = 2, seven trials per tastant). (**C** and **D**) Quantitation of taste responses in the control and T2R5-KO animals; also shown are data for a sweet tastant (acesulfame K). Note the lack of responses in both controls (C) and KO animals (D). Scale bars, 100 μm; error bars are means ± SEM.

the individual basic tastes are represented in the insula by finely tuned cells organized in a precise and spatially ordered gustotopic map, where each taste quality is encoded in its own (segregated) stereotypical cortical field.

The organization of the primary taste cortex appears at first glance to be reminiscent of the somatosensory, auditory, and visual systems, which exhibit spatially organized somatotopic, tonotopic, and retinotopic cortical maps (*17*–*19*). However, the cortical maps for these three sensory modalities reflect smooth transitions across features of sensory space, whereas this is not the case in the taste system. Furthermore, in the somatosensory, auditory, and visual systems, the peripheral receptors display exacting spatial order, whereas in taste, a distributed ensemble of peripheral receptor cells in the tongue—without any spatial organization, but with defined identities—nonetheless converge into a fixed cortical map where neurons with similar response profiles are clustered. Why should taste be represented in a spatial map? We speculate that this organization has an ancient evolutionary, possibly developmental, origin rather than a strictly functional origin. Indeed, the perceptual space to be represented by the taste system is limited to just a handful of qualities; thus, having each basic taste represented in individually segregated fields provides a simple and elegant architectural solution to pattern, wire, and interconnect the ensembles of neurons representing each taste quality.

Our studies suggest that the cortical fields representing the individual basic tastes cover only a small fraction of the insula. What does the rest of the insula do? We found that outside the hot spots, only small numbers of sparsely distributed neurons exhibited significant changes in fluorescence during the window of tastant presentation (fig. S6; see also fig. S4). The same results were observed in animals lacking taste receptor function (fig. S6) and irrespective of the quality of the taste stimulus (including artificial saliva alone); hence, these changes apparently do not represent responses to the individual basic tastes. Therefore, the inter–hot spot regions might be involved in other aspects of taste coding, such as the representation of taste mixes, and thus may

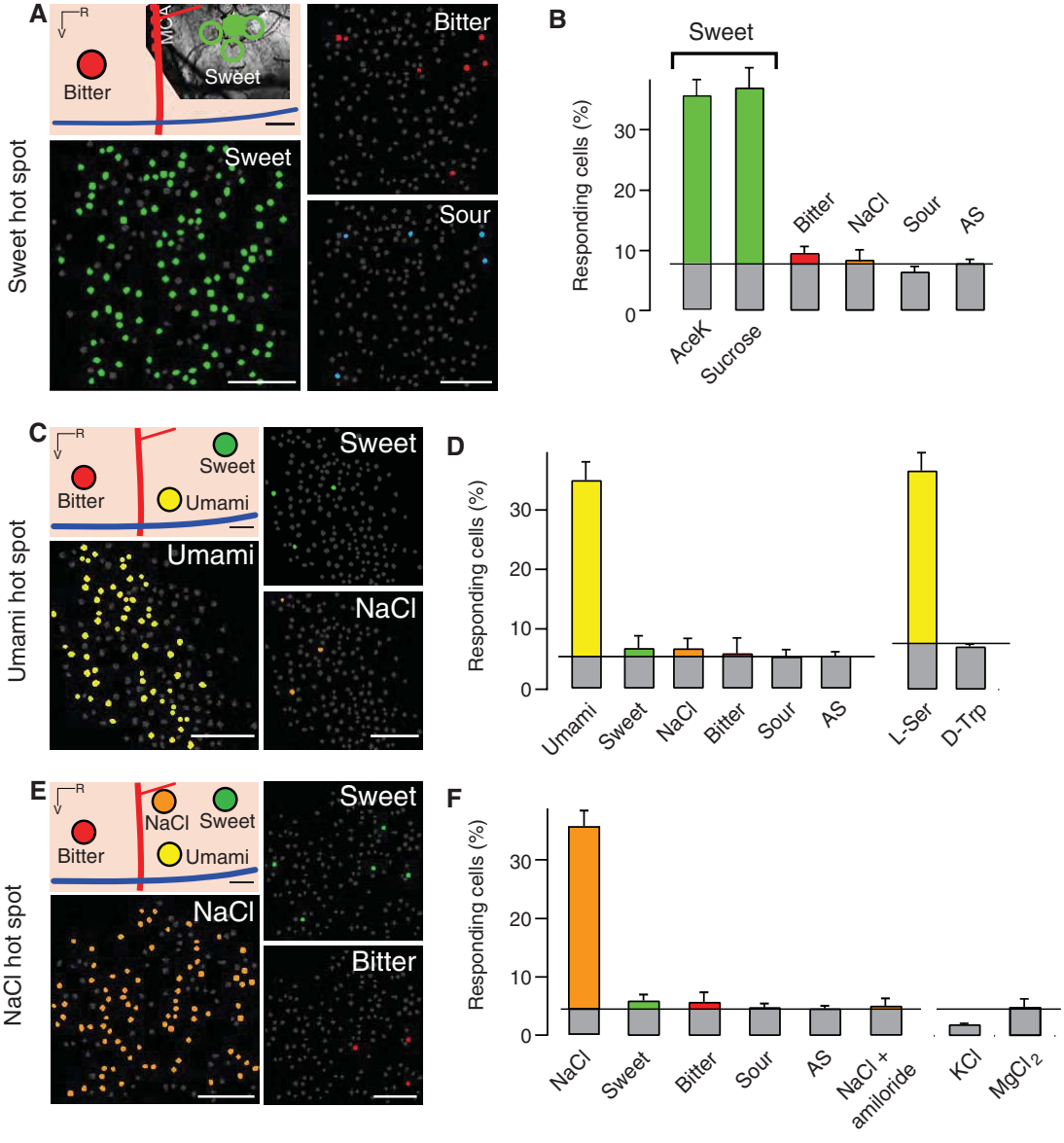

Fig. 4. The basic tastes are represented in a spatial map in the primary taste cortex. (**A** and **B**) Sweet taste is represented in its own cortical field (solid green circle), ~2.5 mm rostrodorsal from the expected location of the bitter hot spot (red circle in upper left illustration). Also shown is the location of the sweet hot spot in three additional animals (open green circles). (A) About 35% of the OGB-labeled neurons in the sweet cortical field respond in multiple trials to sweet taste stimulation of the tongue (green-labeled neurons), but not to other tastes (e.g., bitter and sour). (B) The responses are highly specific for sweet tastants (see also fig. S7), including natural and artificial sweeteners. (**C**) Umami taste is also represented in its own stereotypical hot spot, found ~1 mm caudal and ventral to the expected sweet cortical field (yellow circle). (**D**) Responses are selective for umami tastants, including various L-amino acids, but not to D-amino acids or other taste qualities. (**E**) Low concentrations of sodium salt (100 mM NaCl) are known to activate a unique population of sodium-sensing taste receptor cells (*12*) and are represented in a distinct cortical field (orange circle) ~1 mm equidistant from the expected sweet and umami hot spots. (**F**) Amiloride completely abolishes both the function of the sodium taste receptor and the insular representation of sodium taste. Other salts do not activate the sodium sensor (*12*) and indeed are not represented in the sodium hot spot (e.g., KCl, $MgCl_2$). See fig. S5 for additional details on the sweet, umami, and sodium responses. Scale bars, 100 μm (0.5 mm in the cortex diagrams); error bars are means ± SEM. The hot spots for the different tastes are too far from each other to be imaged on the same animal; reconstructions are based on multiple animals. A minimum of four animals and four trials per animal/per tastant were used to define the sweet (n = 10 animals), umami (n = 5 animals), and sodium (n = 4 animals) cortical fields.

help to code the perception of "flavor" [e.g., responding to several tastes simultaneously (*24*, *26*, *42*)]. In addition, the insular cortex responds to more than just taste, and it is often thought of as a site for multisensory integration (*15*, *42*, *43*). Thus, these areas may participate in the integration of taste with the other senses.

The discovery of a gustotopic map in the mammalian cortex, together with the advent of sophisticated genetic and optical tools (*44*), should now make it possible to experimentally manipulate the taste cortex with exquisite finesse. In future studies, it will also be important to elucidate how taste intensity is encoded in the insular cortex, and to determine whether taste qualities with similar valence project to common targets. Likewise, tracing the connectivity of each of the basic taste qualities to higher brain stations will help decipher how these integrate with other modalities and combine with internal and emotional states to ultimately choreograph taste behaviors (*45*).

References and Notes

1. X. Li *et al.*, *Proc. Natl. Acad. Sci. U.S.A.* **99**, 4692 (2002).
2. G. Nelson *et al.*, *Nature* **416**, 199 (2002).
3. G. Q. Zhao *et al.*, *Cell* **115**, 255 (2003).
4. G. Nelson *et al.*, *Cell* **106**, 381 (2001).
5. E. Adler *et al.*, *Cell* **100**, 693 (2000).
6. J. Chandrashekar *et al.*, *Cell* **100**, 703 (2000).
7. H. Matsunami, J.-P. Montmayeur, L. B. Buck, *Nature* **404**, 601 (2000).
8. K. L. Mueller *et al.*, *Nature* **434**, 225 (2005).
9. J. Chandrashekar, M. A. Hoon, N. J. Ryba, C. S. Zuker, *Nature* **444**, 288 (2006).
10. A. L. Huang *et al.*, *Nature* **442**, 934 (2006).
11. Y. Ishimaru *et al.*, *Proc. Natl. Acad. Sci. U.S.A.* **103**, 12569 (2006).
12. J. Chandrashekar *et al.*, *Nature* **464**, 297 (2010).
13. Y. Zhang *et al.*, *Cell* **112**, 293 (2003).
14. D. A. Yarmolinsky, C. S. Zuker, N. J. Ryba, *Cell* **139**, 234 (2009).
15. S. A. Simon, I. E. de Araujo, R. Gutierrez, M. A. Nicolelis, *Nat. Rev. Neurosci.* **7**, 890 (2006).
16. D. D. Stettler, R. Axel, *Neuron* **63**, 854 (2009).
17. M. M. Merzenich, P. L. Knight, G. L. Roth, *J. Neurophysiol.* **38**, 231 (1975).
18. R. J. Tusa, L. A. Palmer, A. C. Rosenquist, *J. Comp. Neurol.* **177**, 213 (1978).
19. T. A. Woolsey, H. Van der Loos, *Brain Res.* **17**, 205 (1970).
20. R. Accolla, B. Bathellier, C. C. Petersen, A. Carleton, *J. Neurosci.* **27**, 1396 (2007).
21. H. Yoshimura, T. Sugai, M. Fukuda, N. Segami, N. Onoda, *Neuroreport* **15**, 17 (2004).
22. M. Sugita, Y. Shiba, *Science* **309**, 781 (2005).
23. E. S. Soares *et al.*, *Physiol. Behav.* **92**, 629 (2007).
24. J. R. Stapleton, M. L. Lavine, R. L. Wolpert, M. A. Nicolelis, S. A. Simon, *J. Neurosci.* **26**, 4126 (2006).
25. T. Yamamoto, *Prog. Neurobiol.* **23**, 273 (1984).
26. A. Carleton, R. Accolla, S. A. Simon, *Trends Neurosci.* **33**, 326 (2010).
27. D. B. Katz *et al.*, *J. Neurosci.* **28**, 11802 (2008).
28. J. N. Kerr *et al.*, *J. Neurosci.* **27**, 13316 (2007).
29. K. Ohki, S. Chung, Y. H. Ch'ng, P. Kara, R. C. Reid, *Nature* **433**, 597 (2005).
30. C. Stosiek, O. Garaschuk, K. Holthoff, A. Konnerth, *Proc. Natl. Acad. Sci. U.S.A.* **100**, 7319 (2003).
31. C. N. Cearley *et al.*, *Mol. Ther.* **16**, 1710 (2008).
32. See supporting material on *Science* Online.
33. T. Komiyama *et al.*, *Nature* **464**, 1182 (2010).
34. S. V. Wu, M. C. Chen, E. Rozengurt, *Physiol. Genomics* **22**, 139 (2005).
35. K. Iwasaki, T. Kasahara, M. Sato, *Physiol. Behav.* **34**, 531 (1985).
36. We used the monopotassium form of glutamate to prevent confounding activity from a potential sodium taste hot spot (*3*).
37. S. C. Kinnamon, R. F. Margolskee, *Curr. Opin. Neurobiol.* **6**, 506 (1996).
38. T. Arai, T. Ohkuri, K. Yasumatsu, T. Kaga, Y. Ninomiya, *Neuroscience* **165**, 1476 (2010).
39. A. Caicedo, K. N. Kim, S. D. Roper, *J. Physiol.* **544**, 501 (2002).
40. T. A. Gilbertson, J. D. Boughter Jr., H. Zhang, D. V. Smith, *J. Neurosci.* **21**, 4931 (2001).
41. T. Sato, L. M. Beidler, *Chem. Senses* **22**, 287 (1997).
42. D. B. Katz, S. A. Simon, M. A. Nicolelis, *J. Neurosci.* **21**, 4478 (2001).
43. M. Kadohisa, E. T. Rolls, J. V. Verhagen, *Chem. Senses* **30**, 401 (2005).
44. L. Fenno, O. Yizhar, K. Deisseroth, *Annu. Rev. Neurosci.* **34**, 389 (2011).
45. A. Fontanini, D. B. Katz, *Ann. N.Y. Acad. Sci.* **1170**, 403 (2009).

Acknowledgments: We thank A. Devor and Y. Dan for their hospitality and technical help with our early intrinsic imaging attempts, R. Barreto for valuable help with imaging and data analysis, S. Hunter-Smith for help with viral tracing experiments, and R. Axel, K. Scott, D. Steddler, R. Bruno, and members of the Zuker lab for helpful comments. Supported by a Human Frontier Science Program fellowship (X.C.) and by the Intramural Research Program of the National Institute of Dental and Craniofacial Research. C.S.Z. is an investigator of the Howard Hughes Medical Institute.

Supporting Online Material

www.sciencemag.org/cgi/content/full/333/6047/1262/DC1
Materials and Methods
Figs. S1 to S8
References

9 February 2011; accepted 8 July 2011
10.1126/science.1204076

REPORTS

Vacuum-Induced Transparency

Haruka Tanji-Suzuki,[1,2]* Wenlan Chen,[2] Renate Landig,[2] Jonathan Simon,[1] Vladan Vuletić[2]

Photons are excellent information carriers but normally pass through each other without consequence. Engineered interactions between photons would enable applications as varied as quantum information processing and simulation of condensed matter systems. Using an ensemble of cold atoms strongly coupled to an optical cavity, we found that the transmission of light through a medium may be controlled with few photons and even by the electromagnetic vacuum field. The vacuum induces a group delay of 25 nanoseconds on the input optical pulse, corresponding to a light velocity of 1600 meters per second, and a transparency of 40% that increases to 80% when the cavity is filled with 10 photons. This strongly nonlinear effect provides prospects for advanced quantum devices such as photon number–state filters.

The experimental realization of strong coherent interactions between individual photons will enable a variety of applications such as quantum computing (*1*–*3*) and studies of strongly correlated many-body quantum systems (*4*). Two main approaches to generating photon-photon interactions are strong coupling of single emitters to optical cavities (*2*, *3*, *5*–*9*) and electromagnetically induced transparency (EIT) in ensembles of atoms (*10*–*12*). Single emitters strongly coupled to cavities can provide substantial optical nonlinearity at the expense of typically large input-output coupling losses and the technical challenges of trapping and manipulating single particles. EIT in atomic ensembles provides an impressive degree of coherent control in simple, elegant experiments (*12*–*15*), but the nonlinearities achieved so far are relatively weak, requiring (for example) ~500 photons for all-optical switching (*16*). We demonstrate that by using an optical cavity to enhance the EIT control field, the resonant transmission of light through an atomic ensemble can be substantially altered by a few photons and even by the cavity vacuum (*17*, *18*). Because the effect is nonlinear in both control and probe fields at the single-photon level, it should enable advanced quantum optical devices such as photon number–state filters (*19*) and nondestructive photon number–resolving detectors (*20*, *21*). We call the limiting case with no photons initially in the cavity "vacuum-induced transparency" (VIT) (*17*) to distinguish it from recent cavity EIT demonstrations using a single atom with cavity-enhanced absorption and a classical control field containing many photons (*22*, *23*). In contrast, VIT may be realized with only one photon in the entire system.

We experimentally realize Field's original proposal (*17*) to replace the EIT control field by the vacuum field inside a strongly coupled cavity (Fig. 1). In an atomic Λ system $|f\rangle \leftrightarrow |e\rangle \leftrightarrow |g\rangle$ with two stable states $|f\rangle$, $|g\rangle$, the probe beam addresses the $|f\rangle \rightarrow |e\rangle$ transition, whereas the cavity mode is tuned near the $|g\rangle \rightarrow |e\rangle$ transition. A cold atomic ensemble is prepared in the state $|f\rangle$ by optical pumping. VIT for the probe beam can be thought of as arising from a vacuum-induced Raman process where the incoming probe photon is absorbed, quickly emitted into the cavity, then reabsorbed by the ensemble and reemitted

[1]Department of Physics, Harvard University, Cambridge, MA 02138, USA. [2]Department of Physics, MIT-Harvard Center for Ultracold Atoms, and Research Laboratory of Electronics, Massachusetts Institute of Technology, Cambridge, MA 02139, USA.

*To whom correspondence should be addressed. E-mail: haruka.tanji@post.harvard.edu

Supporting Online Material for

A Gustotopic Map of Taste Qualities in the Mammalian Brain

Xiaoke Chen, Mariano Gabitto, Yueqing Peng, Nicholas J. P. Ryba, Charles S. Zuker*

*To whom correspondence should be addressed. E-mail: cz2195@columbia.edu

Published 2 September 2011, *Science* **333**, 1262 (2011)
DOI: 10.1126/science.1204076

This PDF file includes:

Materials and Methods

Animals

Experiments were carried out using 5 - 8 week old C57BL/6J, mT1R2$^{-/-}$ (*S1*) or mT2R5$^{-/-}$ (*S2*) mice; all animal care was in accordance with institutional guidelines. Cortical imaging data were obtained in animals anesthetized with 1.6 mg / g urethane, delivered in two intra-peritoneal injections separated by 30 min. For thalamic recordings and AAV viral injections, animals were anesthetized with ketamine / xylazine (at a ratio of 100 / 10 mg per kg). Supplemental local anesthesia was provided by injection of 2% lidocaine prior to skin incisions; core-body temperature of anesthetized animals was maintained at 37 ˚C using a feedback controlled heating pad.

Recordings and viral tracing of taste-responsive neurons in the thalamus

A small hole was drilled into the skull of 5 - 8 week old C57BL/6J animals at ~0.65 mm from the midline and 2.0 mm caudal to the bregma. A tungsten recording electrode was introduced through this opening and advanced approximately 4.2 mm from the pia into the taste responsive ventromedial posteromedial nucleus of the thalamus [VPM; (*S3*)]. Lingual stimulation and extracellular recordings were as described previously for chorda tympani nerve recordings (*S1, S4*). Signal was amplified, bandpass filtered at 300 - 10, 000 Hz, and digitized. Spikes were identified using a custom Matlab routine that seeks signals that are equal or greater than 4 standard deviations from the baseline. 200 nl of AAV2/Hu11-GFP (*S5*) was pressure injected into the taste-responsive region of the VPM using a nanoliter injector. Two weeks after viral infection, the insular cortex was exposed and DiI was applied to mark the intersection of the middle cerebral artery (MCA) and rhinal veins (RV). The brain was fixed in 4% paraformaldehyde in phosphate buffered saline and sectioned. Sections (100 μm) were counterstained with TO-PRO-3 (1:1000) to highlight cortical layers and imaged for GFP, DiI and TO-PRO-3 fluorescence using confocal microscopy.

Accessing the insular cortex for imaging and recordings

Animals were tracheotomized under 1.6 mg / g urethane anesthesia, and both sides of the hypoglossal nerve were severed to immobilize the tongue. Additional anesthesia was provided using 1-2% isoflurane ventilated through the tracheotomy incision; the mouse's head was secured in a custom-made holder using dental acrylic to eliminate the risk of damaging the taste responsive chorda tympani nerve during surgery. To gain access to the insular cortex, an incision was made to expose the masseter muscle, and the mandible was then retracted to reveal the ventral-lateral surface of the skull; this allowed clear visualization of the lateral olfactory tract, the MCA and RV; as vascular landmarks varied slightly from animal to animal, many imaging fields were explored near the location of the expected hot spots. A custom-made chamber was cemented to the skull (to create a watertight compartment), and a small 1 x 1 mm craniotomy, approximately 2 mm dorsal to the lateral olfactory tract and either anterior or posterior to the MCA (see Fig. 1), was drilled over the insular cortex. After removal of the skull, the chamber was filled with warmed (37 ˚C) artificial cerebrospinal fluid (ACSF): 125 mM NaCl, 5 mM KCl, 10 mM glucose, 10 mM HEPES pH 7.4, 2 mM $CaCl_2$, and 2 mM $MgCl_2$. While hot spots were identified by following vascular landmarks, it should be noted that the relative positions of cortical arteries and veins often varies slightly between animals leading to small variations in the relative location of the hot spots after reconstruction (see for example Fig 2f and 4a). The bitter cortical field was located ~1 mm dorsal to the rhinal veins and ~1 mm posterior to the MCA; the sweet hotspot was approximately 2.5 mm rostro-dorsal to the bitter field; the umami hot spot was approximately 1 mm ventral to the sweet cortical field and the NaCl cortical field was approximately 1 mm from both the sweet and umami hot spots.

For single unit recording, a tungsten electrode (resistance 2.0-4.0 MΩ) was used to isolate individual gustatory neurons in the insular cortex. The electrode was advanced through the dura and into the brain with an electronically controlled micropositioner. Signals were amplified, bandpass filtered at 600-6000 Hz, and digitized with a Neuralynx data acquisition system. A neuron was considered a responder (i.e. to sweet, bitter, sour, umami or salty stimuli) if the increase in spike frequency was statistically significant above the pre-stimulation rate (one-way ANOVA $P < 0.05$); spike activity during the 5

sec window of tastant application was averaged for each trial ($n \geq 6$) and for each of the 5 taste qualities.

Dye Injections

Neurons in layer 2-3 of the insular cortex were bulk-loaded with the calcium-sensitive dye Oregon Green 488 BAPTA-1 AM (OGB-AM) under two-photon microscopy as described previously (*S6-S8*). We used glass pipettes with 5 μm tips to inject a solution containing 0.5 mM OGB-AM, 25 μM sulforhodamine 101, 4 % dimethylsulfoxide and 0.8 % (w/v) Pluronic F-127 in Ca^{2+}/Mg^{2+} free ACSF; the dye solution was maintained at 0 ˚C. Neurons were bulk-loaded over 5 min. by applying 100 - 200 ms pulses of 5 - 10 psi to the pipette to pressure eject dye at several sites approx. 300 μm apart from each other, and 200 - 250 μm below the surface of the insula. This procedure loaded hundreds of cells in an area with a diameter of about 600 μm (see Fig. 1d). After dye injection, the craniotomy was covered with 1.5% agarose in ACSF and sealed using dental acrylic with a No. 0 glass coverslip pre-cut to fit inside the custom chamber; this type of cranial window significantly decreased brain movement (*S7*).

Functional Imaging

Two-photon imaging was carried out using a two-photon microscope with a 40x water immersion objective (IR, N.A. = 0.8). This provided a 350 x 350 μm field of view that was scanned at 2-4 Hz and recorded as a series of 256 x 256 pixel images; we generally used 2 Hz as a compromise between high-quality images and full field imaging. No differences in results or conclusions were seen when imaging at 4 Hz. The excitation wavelength was 810 nm and fluorescence emission was filtered with a 580 dcxr dichroic and hq525/70 m-2p bandpass filter. Taste stimuli were delivered rapidly (> 2 ml / min.) to the entire tongue and oral cavity using a pressure-controlled perfusion system. For all experiments, a 30 s pre-stimulus application of artificial saliva (AS) preceded 10 s exposure to the test tastants and was followed by a 30 s AS wash; inter-trial window was 2 min. Unlike studies in the olfactory, visual, auditory or somatosensory system where the stimuli can be delivered and removed within milliseconds, and dozens of trials readily tested, the need to deliver significant amount of fluid to the tongue, and to thoroughly

remove and wash the oral cavity between trials necessitates long trial times, thus limiting the total number of trials that can be tested in any one experiment. In general, one out of 4 animals could be successfully imaged (failures likely due to problems with damage to brain during surgery, OGB loading the correct cortical fields, difficulties with anesthesia, proper triangulation of vascular landmarks, etc); 4 - 8 trials (typically consisting of a series of 7 different tastants and AS in each trial) were imaged in each cortical field of view. Tastants used in our study were the highest available grade from Sigma and were dissolved in AS (*S1, S4*). Tastants were: 1 mM cycloheximide; 10 mM quinine; 10 mM denatonium benzoate; 30 mM acesulfameK; 300 mM sucrose; 100 mM mono potassium L-glutamate (MPG) + 1 mM inosine monophosphate (IMP); 100 mM L-serine + 1 mM IMP; 100 mM D-tryptophan + 1 mM IMP; 100 mM NaCl (low salt); 100 mM NaCl + 10 μM amiloride; 100 mM KCl; 100 mM MgCl2; 10mM citric acid.

After functional recording, the blood vessel patterns both on the surface of the cortical field of view and in adjacent areas, were imaged as reference points for spatial reconstructions. We also regularly recorded the blood vessel pattern over the entire craniotomy to assist in generating response maps from multiple imaging sites.

Image Analysis

The imaging data were analyzed using custom software written in Matlab. Lateral motion artifacts were corrected using the Image Stabilizer plugin in ImageJ. We then averaged the raw images across the entire t-series (i.e. 140 frames for 70s at a 2 Hz sampling rate) to generate a template used to delineate the outline of the neurons in the imaging field of view. Cell bodies were semi-automatically detected using a fast normalized cross-correlation routine. Briefly, the averaged images were cross-correlated against a kernel with a size approximating that of an average cell; this image map was thresholded to generate a binary mask that demarcated the cell bodies; about 200 neurons were found in a typical field of view (*S9*). Cellular fluorescence intensity (F_t) was calculated for the individual neurons at each time-point by averaging the intensity of pixels falling within the cell boundaries. Mean basal fluorescence (F_o) was assigned to each cell by averaging fluorescence intensity over the first 30 s (before tastant application). The $\Delta F/F$ fluorescence change during tastant stimulation was calculated as $[F_t - F_o] / F_o$ and the

standard deviation of the pre-stimulus baseline determined (σo). Neurons were considered responders when ΔF/F exceeded 3.5 σ_o above F_o for at least two consecutive frames during the 10 s stimulation period (i.e. during the 10 s of tastant application); data were also analyzed using the significantly less stringent criteria of 2.5 and 3.0 standard deviations (see Fig. S7). All routines were built on a GUI software platform in Matlab to provide an interface that allows visualization and manual editing at each step and permits analysis of experiments in minutes. Program is available upon request (Mariano Gabitto <mig2118@columbia.edu>)

References

S1. G. Q. Zhao *et al.*, *Cell* 115, 255 (Oct 31, 2003).

S2. K. L. Mueller *et al.*, *Nature* 434, 225 (Mar 10, 2005).

S3. G. Paxinos, K. B. J. Franklin, *The mouse brain in stereotaxic coordinates* (Academic Press, ed. 3rd Edition, 2007).

S4. G. Nelson *et al.*, *Nature* 416, 199 (Mar 14, 2002).

S5. C. N. Cearley *et al.*, *Mol Ther* 16, 1710 (Oct, 2008).

S6. K. Ohki, S. Chung, Y. H. Ch'ng, P. Kara, R. C. Reid, *Nature* 433, 597 (Feb 10, 2005).

S7. D. D. Stettler, R. Axel, *Neuron* 63, 854 (Sep 24, 2009).

S8. C. Stosiek, O. Garaschuk, K. Holthoff, A. Konnerth, *Proc Natl Acad Sci U S A* 100, 7319 (Jun 10, 2003).

S9. T. Komiyama *et al.*, *Nature* 464, 1182 (Apr 22, 2010).

S10. T. R. Sato, N. W. Gray, Z. F. Mainen, K. Svoboda, *PLoS Biol* 5, e189 (Jul, 2007).

Fig. S1

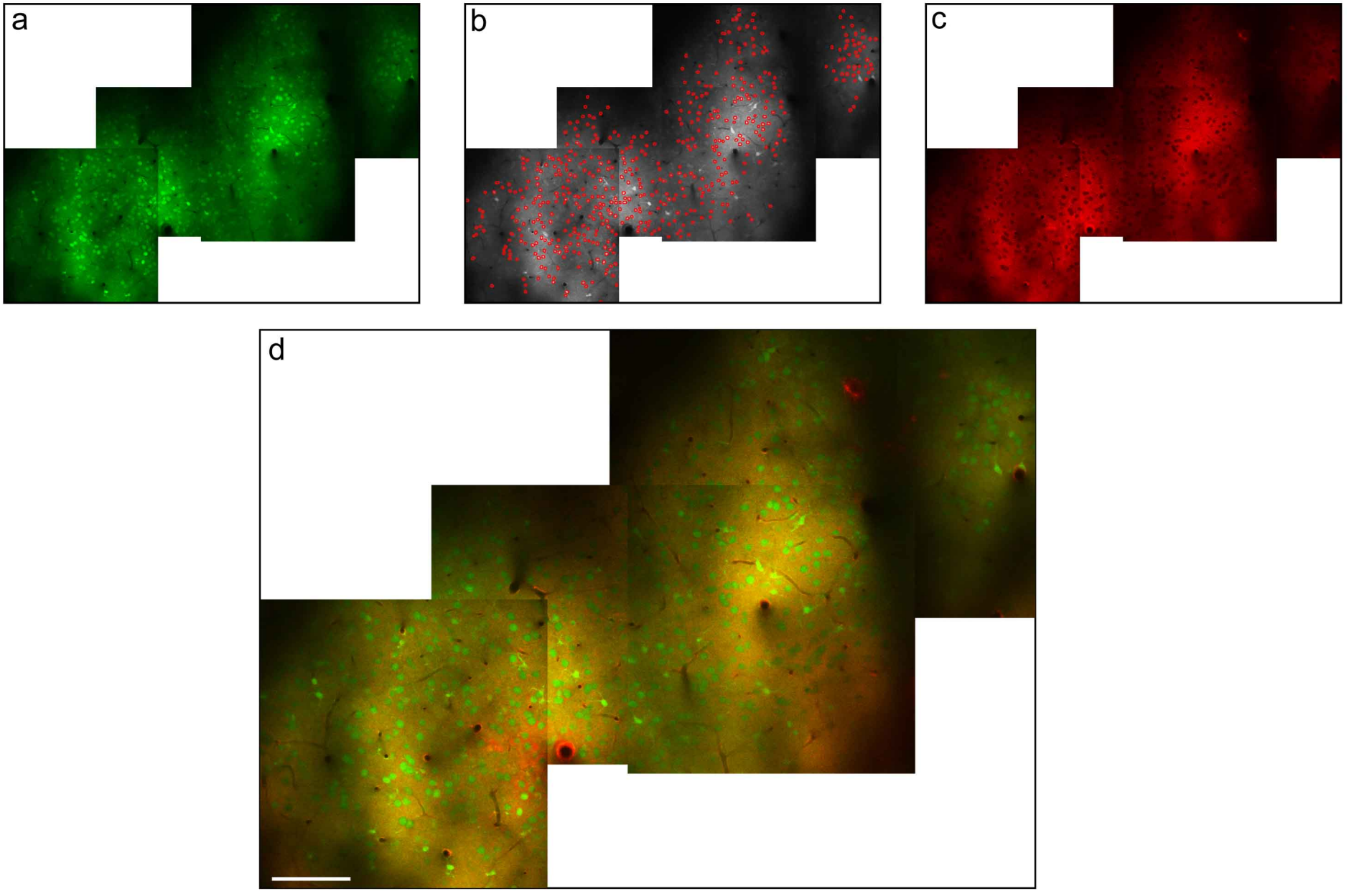

Fig. S1 OGB1-AM labeled neurons in insular cortex

(a) Neurons were loaded with the calcium indicator OGB1-AM as described in Methods. (b) Labeled cells were identified and segmented using a semi-automated fast normalized cross-correlation routine (program available from Mariano Gabitto <mig2118@columbia.edu>). (c) To demonstrate that most neurons picked up the calcium indicator dye, the tissue was independently labeled with the cell impermeant dye Alexa-594 (*S10*). Panel (d) shows the super-imposition of panels (a) and (c); note that most cells were labeled with OGB1-AM; scale bar = 100 μm.

Fig. S2

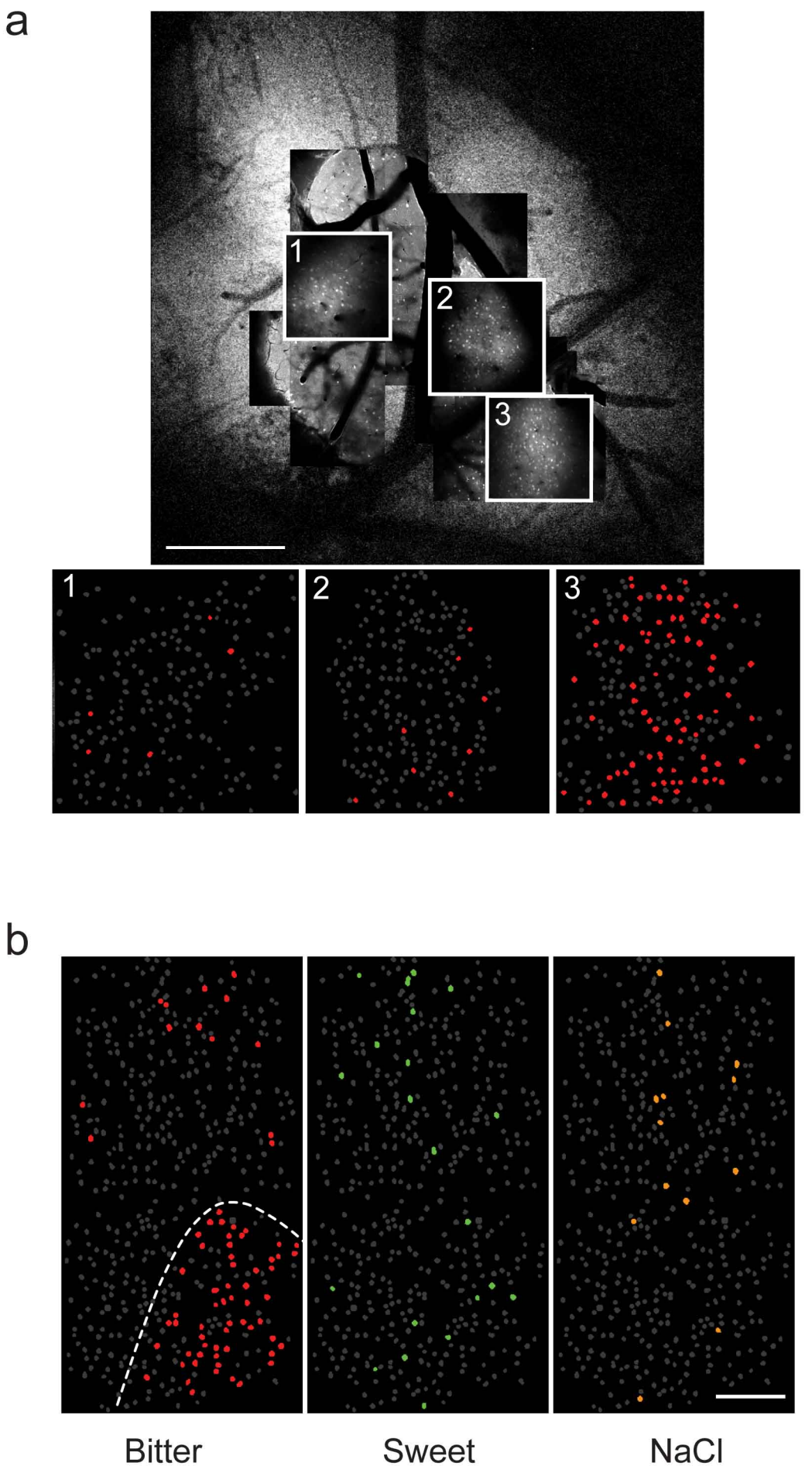

Fig. S2 Montage of imaging fields around the bitter hot spot

Vascular landmarks allow the registering of imaging fields in insular cortex. (a) Shown are 3 fields illustrating the clustering of the bitter-only responsive cells in the bitter hot spot; note the differences between the hot spot (field #3) and the adjacent fields (#1 and 2). (b) Also shown is a 700 x 350 μm field illustrating the sharp boundaries between a hot spot and surrounding cells. Scale bars: panel a = 300 μm, panel b = 100 μm.

Fig. S3

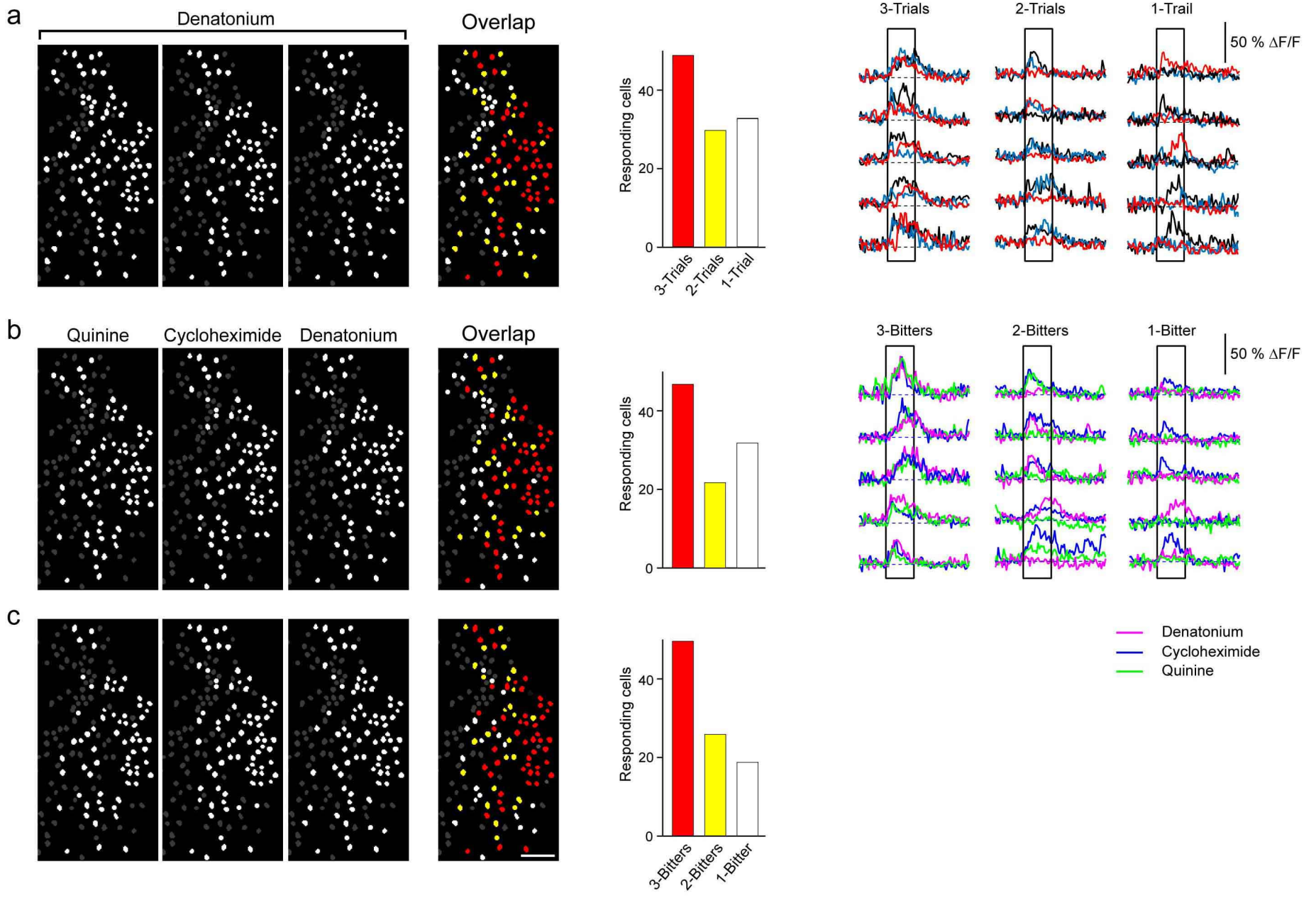
a
Denatonium
Overlap
Responding cells
40
20
0
3-Trials
2-Trials
1-Trial
3-Trials
2-Trials
1-Trail
50 % ΔF/F
b
Quinine
Cycloheximide
Denatonium
Overlap
Responding cells
40
20
0
3-Bitters
2-Bitters
1-Bitter
50 % ΔF/F
Denatonium
Cycloheximide
Quinine
c
Responding cells
40
20
0
3-Bitters
2-Bitters
1-Bitter

Fig. S3 Different bitters are represented in the same cortical field, and activate a similar ensemble of neurons

(a) Responses in the bitter cortical field to 3 separate trials of 10 mM denatonium in the same animal. The rightmost panel and histogram illustrate the number of cells that responded to only 1 trial (white), those that responded to 2 of the trials (yellow) and those that responded to all three trials (red). Note the similarity in the patterns; at least 70% of the neurons responded to 2 of the 3 trials. Also shown are $\Delta F/F$ changes for 15 representative neurons (5 for each group) with each trial illustrated by a different color.

(b) Responses in the bitter cortical field to 3 separate bitters in the same animal (10 mM quinine, 1 mM cycloheximide, 10 mM denatonium). Upper panels illustrate single trials per bitter tastant. The rightmost panel and histogram illustrate the number of cells that responded to only 1 bitter (white), those that responded to 2 of the tastants (yellow) and those that responded to all three (red); $\Delta F/F$ traces are also shown for 5 representative neurons from each group, with each tastant illustrated by a different color. At least 70% of the neurons responded to 2 of the 3 tastants. Note that the variability in trial-to-trial responses to a single bitter (panel a) are similar to the variability seen in trial-to-trial to different bitters (panel b).

(c) Responses as in panel (b), but now each panel shows the cells that responded at least twice to the single bitter tastants and their overlap. Scale bar = 50 μm.

Fig. S4

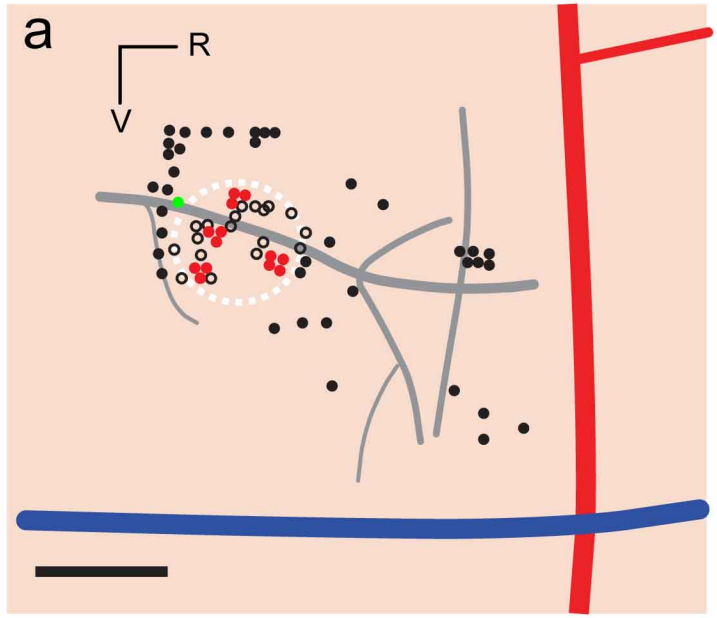
a
R
V

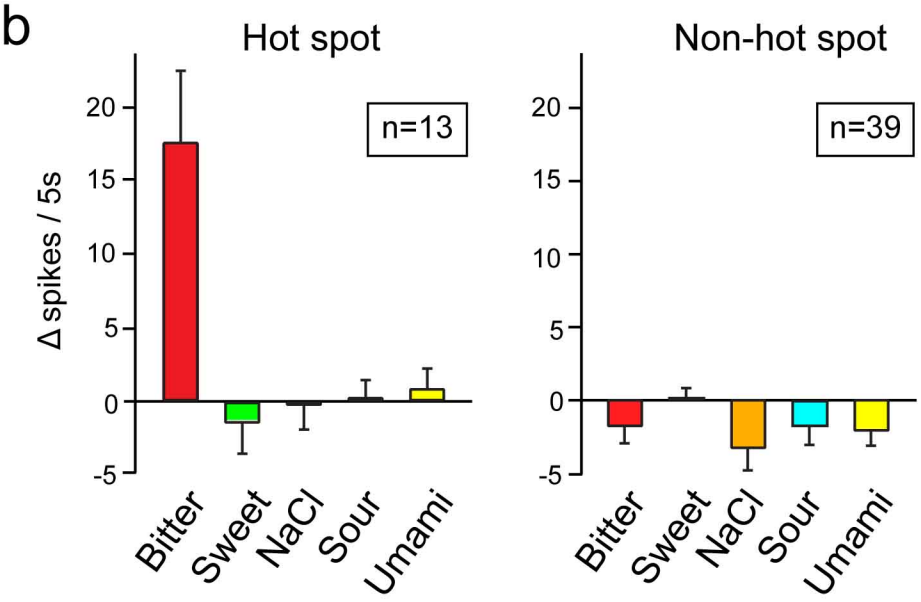
b
Hot spot
Non-hot spot
n=13
n=39
Δ spikes / 5s
Bitter
Sweet
NaCl
Sour
Umami

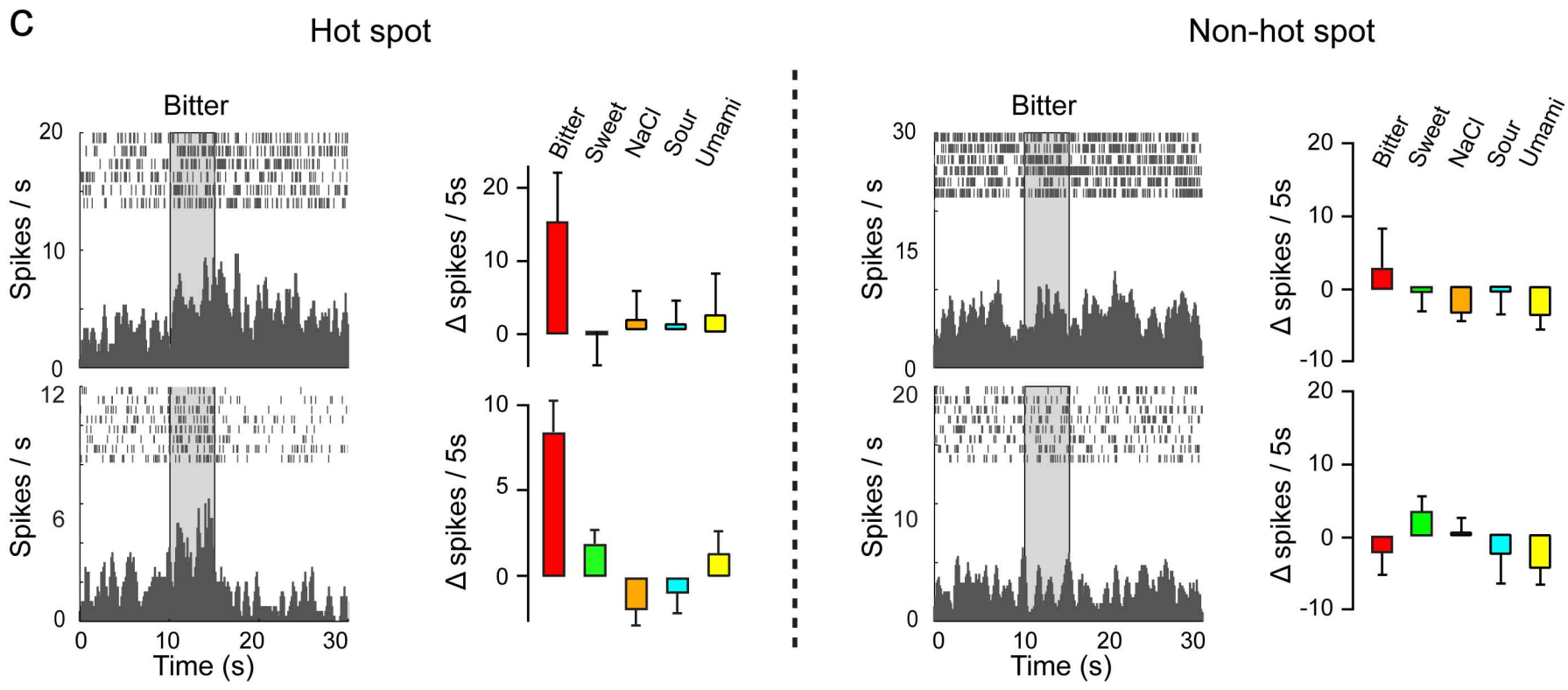
c
Hot spot
Non-hot spot
Bitter
Spikes / s
Time (s)
Δ spikes / 5s
Bitter
Sweet
NaCl
Sour
Umami

Fig. S4 Single unit recordings from the bitter hot spot

To independently validate the segregation of single taste qualities into topographic cortical fields, we also performed single unit recording within (n=4 mice) and outside (n=9 mice) the bitter hot spot. The brain was exposed by surgical craneotony (see Methods), and the responses of cortical neurons inside and outside the hot spot were recorded using standard tungsten electrodes.

(a-b) Just as shown in the 2-photon imaging studies (Fig. 2), responding neurons within the bitter hot spot (demarked by the white dashes, panel a) preferred bitter versus any other taste quality (solid red circles); approximately 30 - 40% of the neurons in the hot spot (solid red versus open circles) displayed responses to taste stimuli (13 of 31 neurons), and these were tuned to bitter (panel b; n = 13). In contrast, of the 39 neurons sampled outside the hot spot, 38 (indicated by the solid black circles) exhibited no statistically significant responses to taste stimuli, and only one (green) showed significant taste responses (to sweet stimuli) above basal spike frequency (one-way ANOVA $P < 0.05$). The relative location of all recorded neurons was determined by triagulating the position of the tungsten electrode to the MCA and RV landmarks (Scale bar = 0.5 mm).

(c) Shown are sample raster plots and peristimulus time histograms (PSTHs) to bitter stimuli from 2 neurons inside and 2 neurons outside the bitter hot spot; the box indicates the time and duration of the stimulus; the PSTHs used a bin of 500 ms. Shown to the right are the summary histograms (n=6 trials) in response to bitter (5 mM quinine), sweet (30 mM acesulfameK), umami (50 mM MPG + 1mM IMP), sour (10mM citric acid) and salt (100 mM NaCl).

Fig. S5

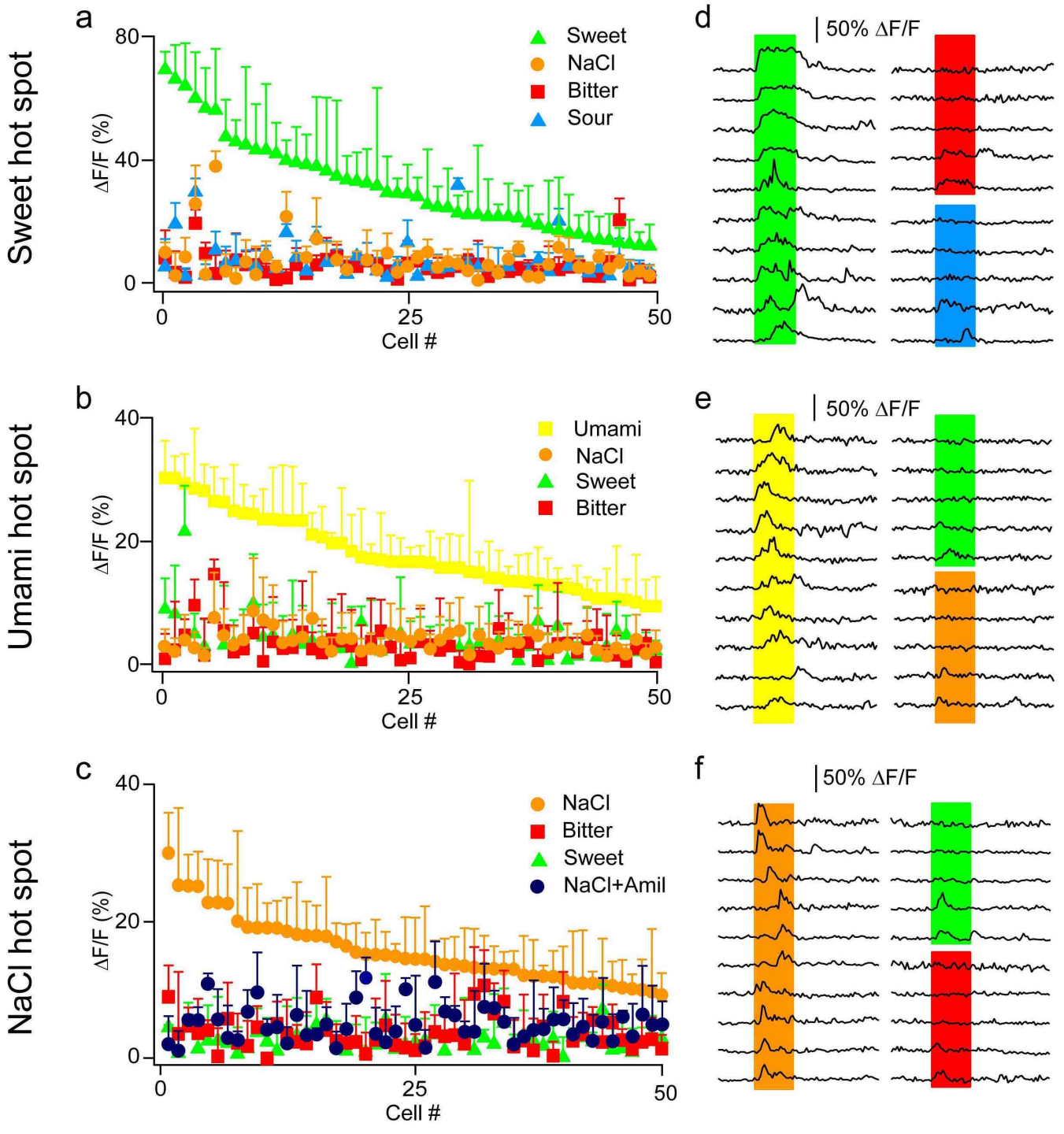
Sweet hot spot
a
80
40
0
ΔF/F (%)
0
25
50
Cell #
Sweet
NaCl
Bitter
Sour
d
50% ΔF/F
Umami hot spot
b
40
20
0
ΔF/F (%)
0
25
50
Cell #
Umami
NaCl
Sweet
Bitter
e
50% ΔF/F
NaCl hot spot
c
40
20
0
ΔF/F (%)
0
25
50
Cell #
NaCl
Bitter
Sweet
NaCl+Amil
f
50% ΔF/F

Fig. S5 Selective responses from neurons in the sweet, umami and sodium-sensing receptive fields.

(a) In the sweet hot spot, sweet responsive neurons are highly tuned to sweet (green) versus other tastants. The graph shows the average peak ΔF/F (rank ordered) of 50 sweet responsive neurons to a wide range of tastants; note the high selectivity for sweet stimuli. (b) Umami responsive neurons are tightly tuned to respond to umami stimuli (yellow). (c) Sodium-sensing neurons exhibit marked selectivity for NaCl (orange) over other tastants. Sweet = 30 mM acesulfameK, Umami = 100 mM MPG + 1mM IMP, NaCl = 100 mM NaCl, Bitter = 10 mM quinine, NaCl+amil = 100 mM NaCl + 10 μM amiloride and Sour = 10 mM citric acid. (d-f) Representative OGB-AM fluorescence changes from different neurons in the (d) sweet, (e) umami and (f) salt hot spots during sweet (green), bitter (red), sour (blue) and NaCl (orange) stimulation. Error bars are mean peak ΔF/F change ± s.e.m from ≥ 4 trials.

Fig. S6

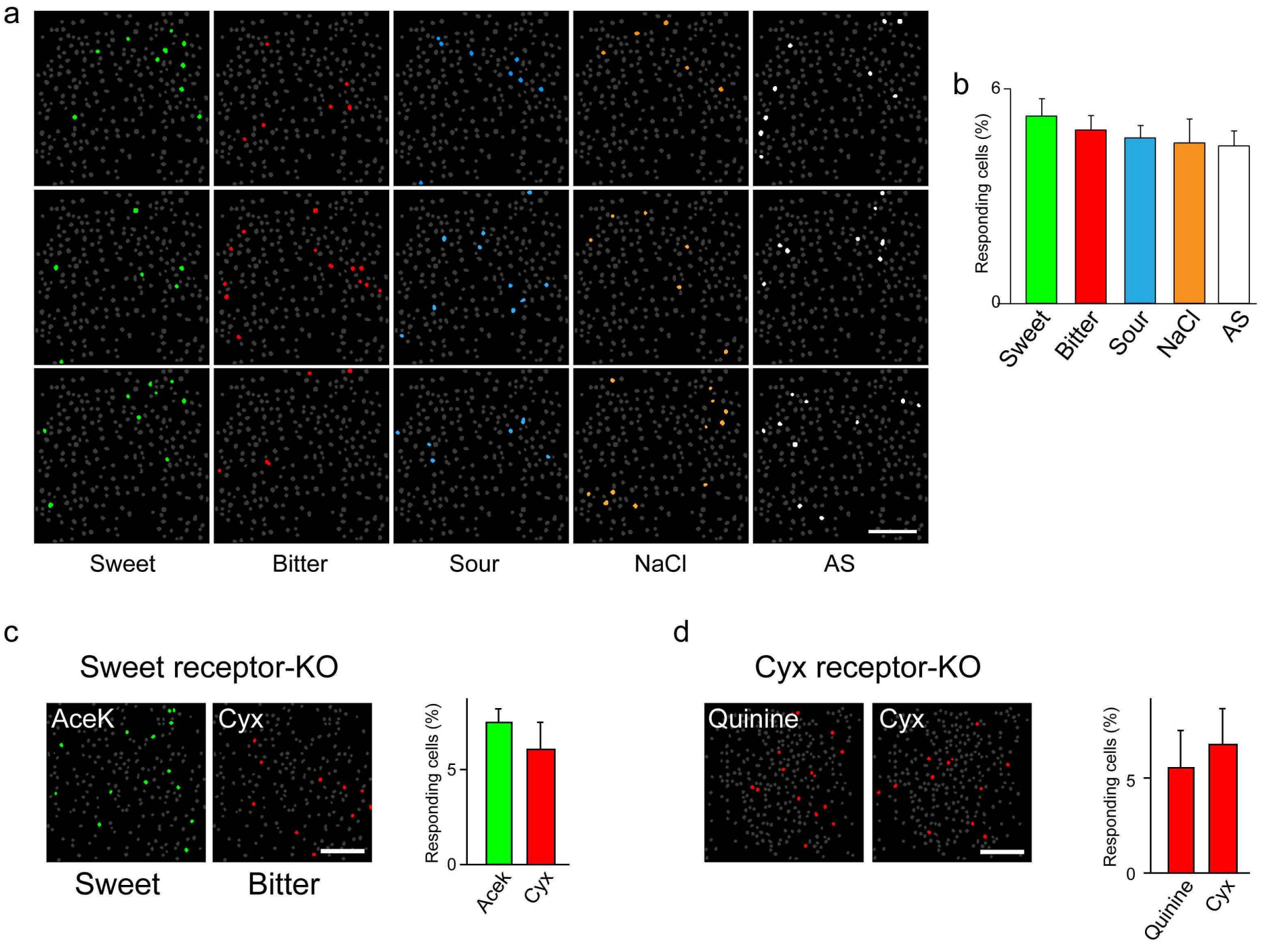
a
Sweet
Bitter
Sour
NaCl
AS
b
Responding cells (%)
6
0
Sweet
Bitter
Sour
NaCl
AS
c
Sweet receptor-KO
AceK
Cyx
Sweet
Bitter
Responding cells (%)
5
0
Acek
Cyx
d
Cyx receptor-KO
Quinine
Cyx
Responding cells (%)
5
0
Quinine
Cyx

Fig. S6 Non-selective responses in the primary taste cortex.

(a) Typically, we can detect sparse patterns of activity in randomly distributed neurons of the insula, with no apparent spatial organization or correlated activity. This activity is seen independent of the nature of the taste stimuli (over most of the insula outside the hot-spots) and is not reproducible between trials (the 3 panels for each tastant represent 3 different trials; note that different subsets of cells are active in each trial). Similar results are also obtained with control tasteless artificial saliva (AS). (b) Histogram data, n = 14. Similar patterns of activity are observed in the primary taste cortex of mice lacking specific taste receptor function. Hence, this type of neural firing cannot represent a taste as it remains in mice that cannot taste. (c) Mice lacking sweet taste receptor function (T1R2-KO) still exhibit equivalent levels of neural firing when exposed to sweet (acesulfameK, 30 mM) or bitter (cycloheximide, 1mM) tastants; mean ± s.e.m, n = 3 animals. (d) T2R5-KO mice lacking the bitter receptor for cycloheximide still exhibit the same patterns of sparse, random activity when exposed to cycloheximide (1 mM) or to other bitter tastants (e.g. 10 mM quinine; n = 5 animals); scale bars = 100 μm.

Fig. S7

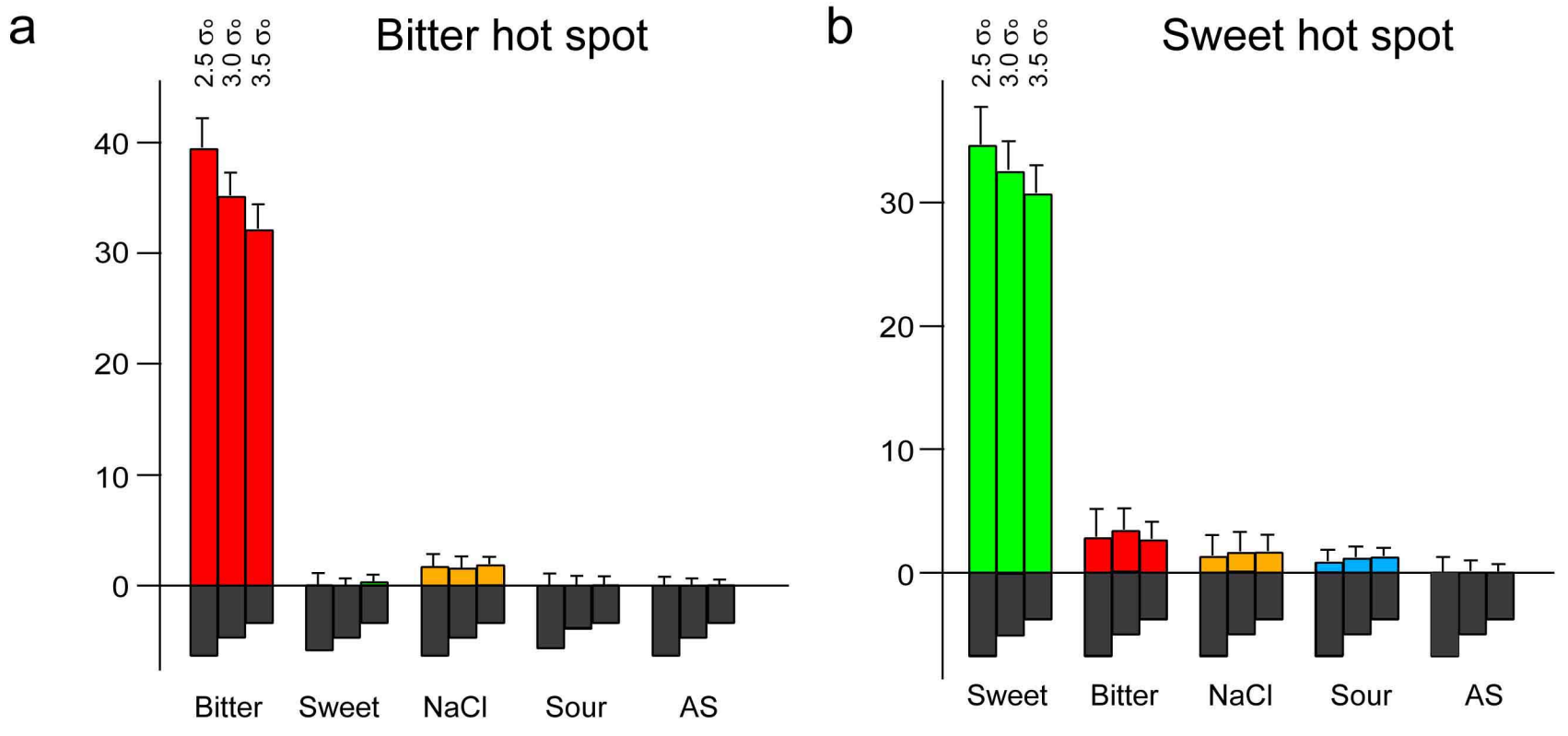
a
Bitter hot spot
2.5 σ₀
3.0 σ₀
3.5 σ₀
40
30
20
10
0
Bitter
Sweet
NaCl
Sour
AS
b
Sweet hot spot
2.5 σ₀
3.0 σ₀
3.5 σ₀
30
20
10
0
Sweet
Bitter
NaCl
Sour
AS

Fig. S7 The basic tastes are represented by neurons selective for their preferred taste quality

Neurons in the bitter (a) and sweet (b) hot spots responded selectively to their preferred but not to other taste stimuli (see methods for details) (n = 4). Data were analyzed as described in methods, but responders were identified using 3 different threshold criteria: 2.5, 3.0 or 3.5 standard deviations above baseline. Although there were small differences in the number of "responding cells" between conditions (compare bars), no differences in their organization into gustotopic clusters, or tastant selectivity were observed.

Fig. S8

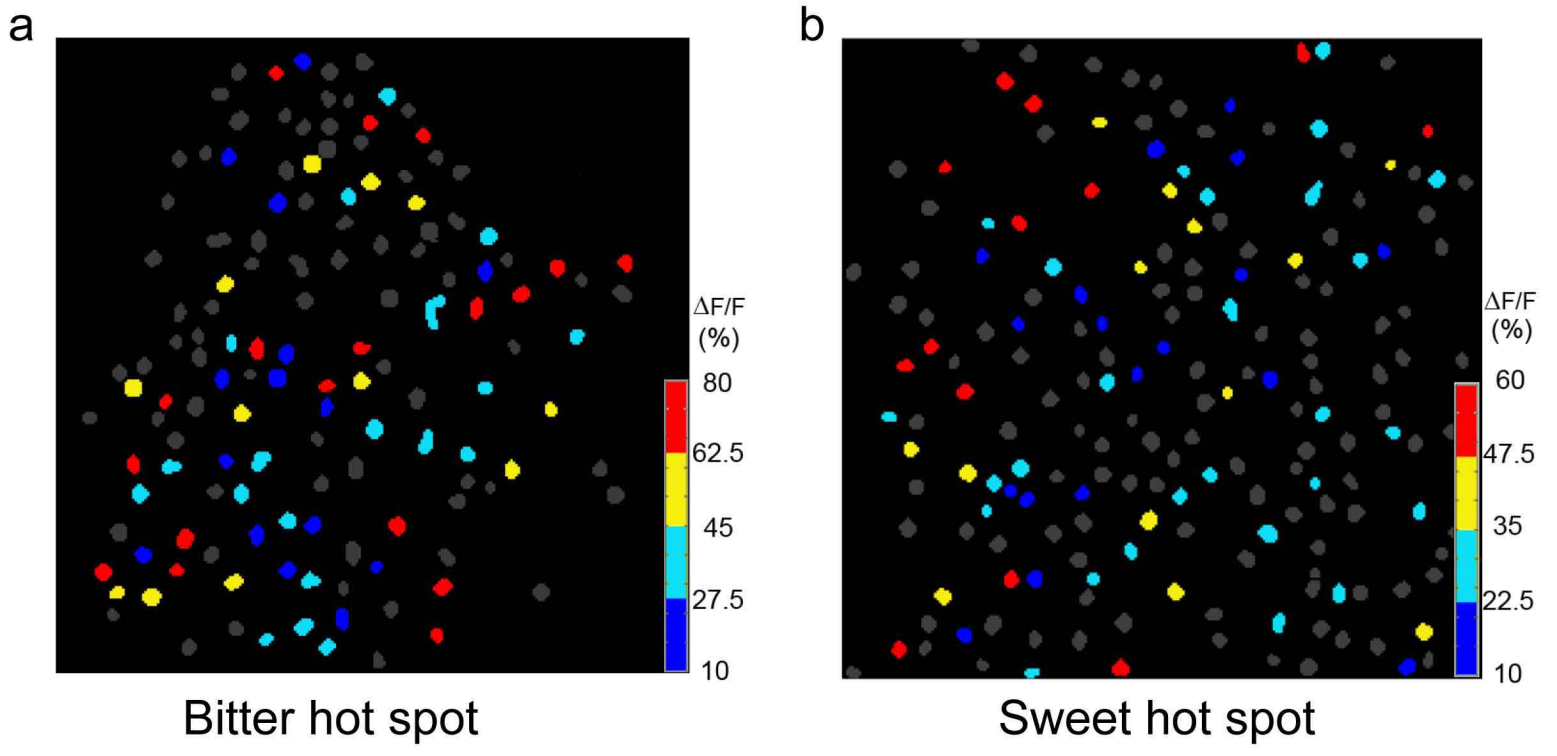
a
ΔF/F
(%)
80
62.5
45
27.5
10
Bitter hot spot
b
ΔF/F
(%)
60
47.5
35
22.5
10
Sweet hot spot

Fig. S8 Cells within a hot spot are not organized according to their response magnitude

(a) Neurons in the bitter hot spot were color-coded according to their response amplitude. Dark blue: ΔF/F 10-27.5%, Pale blue: ΔF/F 27.5-45%, yellow: ΔF/F 45-62.5%, red: ΔF/F 62.5-80%. Note the lack of any microstructure in their organization; similar results were obtained in multiple animals (n = 4). (b) Neurons in the sweet hot spot were also color-coded according to their response amplitude. Dark blue: ΔF/F 10-22.5%, Pale blue: ΔF/F 22.5-35%, yellow: ΔF/F 35-47.5%, red: ΔF/F 47.5-60%. Note the lack of any microstructure in their organization; similar results were obtained in multiple animals (n = 3).